Title
Adaptive Control for Conventional Modes of Operation of MEMS Gyroscopes

Authors
Park, Park
Horowitz, Roberto
Tan, Chin-woo

Publication Date
2002-03-01

CALIFORNIA PATH PROGRAM
INSTITUTE OF TRANSPORTATION STUDIES
UNIVERSITY OF CALIFORNIA, BERKELEY

Adaptive Control for Conventional Modes of Operation of MEMS Gyroscopes

Sungsu Park, Roberto Horowitz, Chin-woo Tan
University of California, Berkeley

California PATH Research Report
UCB-ITS-PRR-2002-10

This work was performed as part of the California PATH Program of the University of California, in cooperation with the State of California Business, Transportation, and Housing Agency, Department of Transportation; and the United States Department of Transportation, Federal Highway Administration.

Report for MOU 329

March 2002

ISSN 1055-1425

Adaptive Control for Conventional Modes of Operation of MEMS Gyroscopes

Sungsu Park
Roberto Horowitz

Department of Mechanical Engineering
University of California, Berkeley
{spark, horowitz}@newton.berkeley.edu

Chin-Woo Tan

California PATH
University of California, Berkeley
tan@robotics.eecs.berkeley.edu

MOU 329

Abstract

This report presents adaptive control algorithms for conventional modes of operation of MEMS z-axis gyroscopes. In an open-loop mode, an off-line self-calibration scheme is proposed for estimating fabrication imperfections and enhancing the performance of a gyroscope operating in open-loop mode. This scheme can be implemented during the initial calibration stage when the gyroscope is turned on, or at regular calibration sessions, which may be performed periodically. An adaptive add-on control scheme is also proposed for a closed-loop mode of operation. This scheme is realized by adding an outer loop to a conventional force-balancing scheme that includes a parameter estimation algorithm. This parameter adaptation algorithm estimates the angular rate, identifies and compensates the quadrature error, and may permit on-line automatic mode tuning. The convergence and resolution analysis show that the proposed adaptive add-on control scheme prevents the angular rate estimate from being contaminated by the quadrature error, while keeping ideal resolution performance of a conventional force-balancing scheme.

1. Introduction

Gyroscopes are commonly used sensors for measuring angular velocity in many areas of applications such as navigation, homing, and control stabilization. Although, conventional rotating wheel, fiber optic and ring laser gyroscopes have dominated a wide range of applications, they are too large and, most often too expensive to be used in most emerging applications.

Recent advances in micro-machining technology have made the design and fabrication of MEMS (Micro-Electro-Mechanical Systems) gyroscopes possible, which are several orders of magnitude smaller than conventional mechanical gyroscopes, and can be fabricated in large quantities by batch processes, potentially reducing fabrication cost significantly. The emergence of MEMS gyroscopes is opening up new market opportunities and applications in the area of low-cost to medium performance inertial devices, including consumer electronics such as virtual reality, video games, 3D mouse and camcorder image stabilization; automotive applications such as ride stabilization, rollover detection and other vehicle safety systems; GPS augmentation such as MEMS inertial navigation sensor imbedded GPS; as well as a wide range of new military applications such as micro airplanes and satellite controls. The design and fabrication of MEMS gyroscopes has been the subject of extensive research over the past few years. [1] contains a comprehensive review of previous efforts in developing high quality cost-effective gyroscopes.

Most MEMS gyroscopes are vibratory rate gyroscopes that have structures fabricated on polysilicon or crystal silicon, and their mechanical main component is a two degree-of-freedom vibrating structure, which is capable of oscillating on two directions in a plane. Their operating principle is based on the Coriolis effect [1]. When the gyroscope is subjected to an angular velocity, the Coriolis effect transfers energy from one vibrating mode to another. The response of the second vibrating mode provides information about the resultant angular motion. This energy transfer is highly efficient when the natural frequency of oscillation of the two vibrating modes is the same and the modes are nearly un-damped. Ideally in the conventional mode of operation, the vibrating modes of a MEMS gyroscope

are supposed to remain mechanically un-coupled, their natural frequencies should be matched, and the gyroscope's output should only be sensitive to angular velocity. In practice, however, fabrication imperfections and environment variations are always present, resulting in a frequency of oscillation mismatch between the two vibrating modes and the presence of linear dissipative forces with time-varying damping coefficients. MEMS gyroscopes are also sensitive to fabrication imperfections. Common fabrication steps of MEMS gyroscopes include bulk micromachining, wafer-to-wafer bonding, surface micromachining, and high aspect ratio micromachining. Each of these fabrication steps involves multiple process steps such as deposition, etching and patterning of materials. Depending on the technology used, different numbers of steps may be involved in the fabrication of a MEMS gyroscope, and different fabrication tolerances can be achieved. Thus, small imperfections always occur during the fabrication process. Fabrication imperfections result in a coupling between the two mechanical vibration modes through off-diagonal terms in the stiffness and damping matrices. These imperfections degrade the gyroscope's performance and cause an erroneous output. As a consequence, some kind of control is essential for improving the performance and stability of MEMS gyroscopes, by effectively canceling "parasitic" effects.

Traditionally, mechanical or electrical balancing has been used to cancel parasitic effects [2,3,4], which is referred to as the open-loop mode of operation. Although this procedure reduces the effect of a certain amount of imperfections, it is time consuming, expensive and difficult to perform on small, nail-size (*mm* level) gyroscopes.

Two feedback control methods have been presented in the literature that compensate fabrication imperfections and measure angular velocity in a closed-loop mode of operation. One is a Kalman filter based preview control [5] and the other is a recently published force-balancing feedback control scheme using sigma-delta modulation [6]. Although these feedback control techniques increase the bandwidth and dynamic range of the gyroscope beyond the open-loop mode of operation, they still are sensitive to parameter variations, and angular rate estimate may be contaminated by the quadrature error.

The objective of this report is to develop adaptive control algorithms for operating a MEMS gyroscope in an ideal conventional mode environment. For an open-loop mode of operation, an off-line self-calibration scheme is proposed for initial estimation and compensation of fabrication imperfections. For a closed-loop mode of operation, an adaptive add-on control scheme is proposed. This adaptive algorithm estimates the angular rate and, at the same time, identifies and compensates quadrature error, and may permit on-line automatic mode tuning.

In the next sections, the dynamics of MEMS gyroscopes is developed and analyzed, by taking into account the effect of fabrication imperfections. The open-loop mode of operation is reviewed and an off-line self calibration scheme is proposed in section 3. An adaptive add-on control approach is developed as an extension of conventional force-balancing control scheme, and the convergence and resolution analysis of the proposed adaptive add-on controlled gyroscope is presented in section 4. Finally, computer simulations are performed in section 5.

2. Dynamics of MEMS Gyroscopes

A typical MEMS vibratory gyroscope configuration includes a proof mass suspended by spring suspensions, and electrostatic actuations and sensing mechanisms for forcing an oscillatory motion and sensing the position and velocity of the proof mass. These mechanical components can be modeled as a multi-degree-of-freedom mass, spring and damper system. The mass in a vibratory gyroscope is generally constrained to move either linearly or angularly. In this report, only linear vibratory gyroscopes are discussed. However, most of the results of this report are applicable to angular vibratory gyroscopes as well. To derive the gyroscope's dynamic equations of motion, two coordinate systems are introduced: the inertial frame, which is fixed in an inertial space, and the gyro frame, which is fixed to the rotation platform. Figure 1 shows a simplified model of a MEMS gyroscope having two degrees of freedom in the associated Cartesian reference frames.

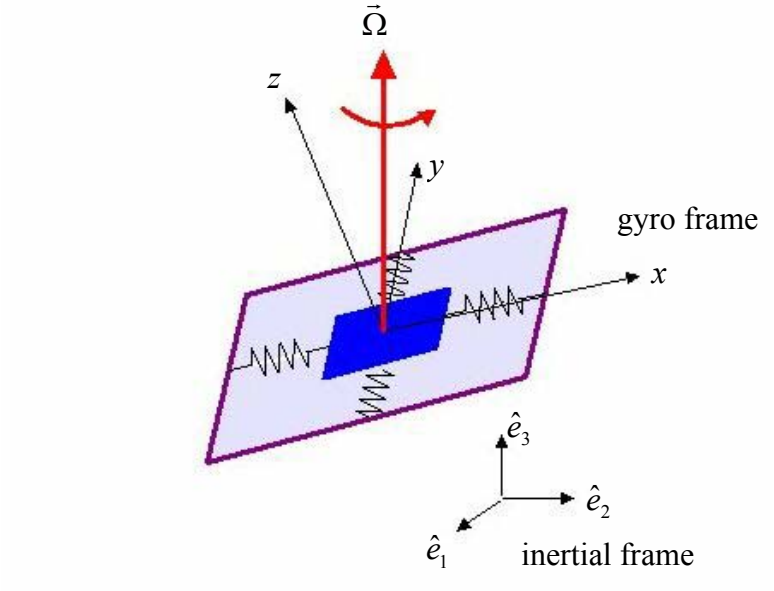

Figure 1. A model of a (planar vibratory) MEMS z-axis gyroscope

Assume that the gyro frame $\{g\}$ is rotated with respect to inertial frame $\{e\}$ by the angular velocity vector ${}^{e}\vec{\Omega}^{g}$, then the equation of the motion of the proof mass of the gyroscope is described as

$$\vec{f} = m\left({}^{e}\frac{d^2\vec{R}_0}{dt^2} + {}^{g}\frac{d^2\vec{r}}{dt^2} + 2\,{}^{e}\vec{\Omega}^{g} \times {}^{g}\frac{d\vec{r}}{dt} + {}^{g}\frac{d\,{}^{e}\vec{\Omega}^{g}}{dt} \times \vec{r} + {}^{e}\vec{\Omega}^{g} \times ({}^{e}\vec{\Omega}^{g} \times \vec{r}) \right) \qquad (1)$$

where $\vec{R}_0$ is the position vector of the origin of the gyro frame with respect to the origin of the inertial frame, $\vec{r}$ is a position vector of the proof mass with respect to the origin of the gyro frame, and $\frac{{}^{a}d(\vec{b})}{dt}$ denotes the time derivative of a vector $\vec{b}$ in the frame $\{a\}$. $\vec{f}$ is a total applied force to the proof mass, which includes spring, damping and control forces. The first term of the equation (1) is the linear acceleration of the gyro frame with respect to the inertial frame and the second term is a linear acceleration of the mass in the gyro frame. The third term is the Coriolis acceleration, which appears only if the equations of motion

are written in the non-inertial frame. The fourth and fifth terms are respectively the linear acceleration due to angular acceleration and the centrifugal acceleration.

If one wants to measure the component of the angular velocity along the *z*-axis, the motion of the proof mass can be constrained to be only along the *x*-*y* plane by making the spring stiffness in the *z* direction much larger than in the *x* and *y* directions. Assuming that the measured angular rate is almost constant over a long enough time interval and that linear accelerations are cancelled out, either as an offset from the output response or by applying counter-control forces, the equations of motion of a gyroscope simplify as follows.

$$\begin{aligned} m\ddot{x} + d_1\dot{x} + (k_1 - m(\Omega_y^2 + \Omega_z^2))x + m\Omega_x\Omega_y y &= \tau_x + 2m\Omega_z\dot{y} \\ m\ddot{y} + d_2\dot{y} + (k_2 - m(\Omega_x^2 + \Omega_z^2))y + m\Omega_x\Omega_y x &= \tau_x - 2m\Omega_z\dot{x} \end{aligned} \tag{2}$$

where *x* and *y* are the coordinates of the proof mass relative to the gyro frame, $d_{1,2}$, $k_{1,2}$ are damping and spring coefficients, $\Omega_{x,y,z}$ are the angular velocity components along each axis of the gyro frame and $\tau_{x,y}$ are control forces. The two last terms in equation (2), $2m\Omega_z\dot{x}$ and $2m\Omega_z\dot{y}$, are due to the Coriolis forces and are the terms which are used to measure the angular rate Ω_z. As seen in equation (2), in an ideal gyroscope, only the component of the angular rate along the *z*-axis, Ω_z, causes a dynamic coupling between the *x* and *y* axes, under the assumption that $\Omega_x^2 \approx \Omega_y^2 \approx \Omega_x\Omega_y \approx 0$. In practice, however, small fabrication imperfections always occur, and also cause dynamic coupling between the *x* and *y* axes through the asymmetric spring and damping terms. These are major factors which limit the performance of MEMS gyroscopes

Taking into account fabrication imperfections, the dynamic equations (2) are modified as follows [7].

$$\begin{aligned} m\ddot{x} + d_{xx}\dot{x} + d_{xy}\dot{y} + k_{xx}x + k_{xy}y &= \tau_x + 2m\Omega_z\dot{y} \\ m\ddot{y} + d_{xy}\dot{x} + d_{yy}\dot{y} + k_{xy}x + k_{yy}y &= \tau_y - 2m\Omega_z\dot{x} \end{aligned} \tag{3}$$

Equation (3) is the governing equation for a *z*-axis MEMS gyroscope. Fabrication imperfections contribute mainly to the asymmetric spring and damping terms, k_{xy} and d_{xy}. Therefore these terms are unknown, but can be assumed to be small. The *x* and *y* axes spring and damping terms are mostly known, but have small unknown variations from their nominal values. The proof mass can be determined very accurately. However, even if there are small-unknown variations in the proof mass, this is not a problem, because equation (3) can be scaled by the proof mass. The components of angular rate along *x* and *y* axes are absorbed as part of the spring terms as unknown variations. Note that the spring coefficients k_{xx} and k_{yy} also include the electrostatic spring softness.

Non-dimensionalizing the equations of motion of a gyroscope is useful because the numerical simulation is easy, even under the existence of large two time-scales differences in gyroscope dynamics. One time scale is defined by the resonant natural frequency of the gyroscope, $\sqrt{k_{xx}/m}$, the other by the applied angular rate Ω_z. Nondimensionalization also produces a unified mathematical formulation for a large variety of gyroscope designs. In this report, controllers will be designed based on non-dimensional equations. The realization to a dimensional control for the specific gyroscope can be easily accomplished by multiplying the dimensionalizing parameters by the non-dimensional controller parameters. Based on m, q_0 and ω_{n}, which are a reference mass, length and natural resonance frequency respectively, where *m* is a proof mass of the gyroscope, the non-dimensionalization of equation (3) can be done as follows:

$$\begin{aligned} \ddot{x} + \frac{\omega_x}{Q_x}\dot{x} + d_{xy}\dot{y} + \omega_x^2 x + \omega_{xy} y &= \tau_x + 2\Omega_z \dot{y} \\ \ddot{y} + d_{xy}\dot{x} + \frac{\omega_y}{Q_y}\dot{y} + \omega_{xy} x + \omega_y^2 y &= \tau_y - 2\Omega_z \dot{x} \end{aligned} \tag{4}$$

where Q_x and Q_y are respectively the x and y axis quality factor, $\omega_x = \sqrt{k_{xx}/(m\omega_0^2)}$, $\omega_y = \sqrt{k_{yy}/(m\omega_0^2)}$, $\omega_{xy} = k_{xy}/(m\omega_0^2)$, $d_{xy} \leftarrow d_{xy}/(m\omega_0)$, $\Omega_z \leftarrow \Omega_z/\omega_0$, $\tau_x \leftarrow \tau_x/(m\omega_0^2 q_0)$ and $\tau_y \leftarrow \tau_y/(m\omega_0^2 q_0)$. The natural frequency of the x or y axis can be used to define the nondimensionalizing parameter ω_0. Since the usual displacement range of the MEMS gyroscope in each axis is sub-micrometer level, it is reasonable to choose $1\,\mu$m as a reference length q_0 . Considering that the usual natural frequency of each of the axis of a vibratory MEMS gyroscope is in the *KHz* range, while the applied angular rate may be in the degrees per second or degrees per hour range, the non-dimensional angular rate that we want to estimate is respectively in the range of 10^{-4} or 10^{-10}!

The conventional mode of operation of a MEMS z-axis gyroscope can be understood by considering the effect of the Coriolis acceleration term on the gyroscope dynamics. The conventional mode of operation reduces to driving one of the modes of the gyroscope into a known oscillatory motion and then detecting the Coriolis acceleration coupling along the sense mode of vibration, which is orthogonal to the driven mode. The response of the sense mode of vibration provides information about the applied angular velocity. Conventional mode of operation is classified by an open-loop mode and a closed-loop mode.

3. Open-loop Mode of Operation

3.1 Operation Strategy and Discussion

Most MEMS gyroscopes are currently operated in the so-called open-loop mode. Consider again the nondimensional equation of motion (4). In the open loop mode of operation, the proof mass is driven into a constant amplitude oscillatory motion along the x-axis (drive

axis) by the *x*-axis control τ_x. When the gyroscope is subjected to an angular rotation, a Coriolis inertial specific force, $-2\Omega_z\dot{x}$, is generated along the *y*-axis (sense axis), whose magnitude is proportional to the oscillation velocity of the drive axis and the magnitude of *z*-axis component of angular rate. This force excites the proof mass into an oscillatory motion along the *y*-axis, and its magnitude is amplified according to the mechanical quality factor (*Q*-factor). This amplified oscillation is demodulated into a signal that is proportional to the input angular rate. Mathematically speaking, the process of open-loop mode of operation is described as follows:

$$x = X_0 \sin(\omega_x t)$$
$$\ddot{y} + \frac{\omega_y}{Q_y}\dot{y} + \omega_y^2 y = \tau_y - \omega_{xy}x - (d_{xy} + 2\Omega_z)\dot{x} \tag{5}$$

where X_0 is the amplitude of *x*-axis oscillation, ω_x and ω_y are resonant frequencies of both axes, and Q_y is the quality factor of the sense axis. The term open-loop mode of operation arises from the fact that no feedback control action is employed on the sense axis (*y*-axis).

As seen in equation (5), there are three forcing terms in the *y*-axis dynamics: the control τ_y, the modulated forcing term due to asymmetric spring constant which is called the quadrature error ω_{xy}, the Coriolis term, and the asymmetric damping d_{xy}. The quadrature error, ω_{xy}, is due to fabrication imperfections and is one source of zero-rate output (ZRO). Cancellation of this effect may be possible because there is a 90^0 phase difference between this term and the coupling Coriolis acceleration, although the exact phase must be known. However, the effect of the asymmetric damping term is not distinguishable from the Coriolis acceleration term. Thus, this term creates an inherent ZRO.

When the quadrature error is cancelled ideally by the sense axis control τ_y, and there is no asymmetric damping, the scale factor between the amplitude of sense axis oscillation Y_0 and the angular rate is given by

$$\left|\frac{Y_0}{\Omega_{z0}}\right| = \frac{2X_0(\omega_x \pm \delta)}{\sqrt{\left(\frac{(\omega_x \pm \delta)\omega_y}{Q_y}\right)^2 + \left((\omega_y^2 - (\omega_x \pm \delta)\right)^2}} \tag{6}$$

where it is assumed that $\Omega_z = \Omega_{z0}\cos(\delta\ t)$, and δ is the angular rate excitation frequency whose value is $\delta << \omega_x$. If the quality factor is not changing, the angular rate can be determined by simply measuring the magnitude of steady state oscillations of the proof mass in the sense axis. Clearly, the static sensitivity is maximum when the resonant frequencies of the drive and sense axes are exactly matched ($\omega_x = \omega_y = \omega_n$). When these two resonant frequencies coincide, the static scale factor equation is

$$\left|\frac{Y_0}{\Omega_z}\right| = \frac{2X_0 Q_y}{\omega_n} \tag{7}$$

In the open loop mode, the response to a change in the angular rate is not instantaneous, since time is required for the amplitude of the sense mode to reach its steady state value. With matched sense and drive resonant modes, the time constant associated with this amplitude build up is equal to $\frac{2Q_y}{\omega_n}$. This response time limits the bandwidth of the sensor to a few hertz. To attain a larger open-loop bandwidth, gyroscopes can be operated with a resonance frequency mismatch in the sense and drive modes, or with an increased resonant frequency, or a reduced quality factor. However, all these approaches must be done at a cost of reduced sensitivity.

Since the quality factor is typically large, the sense axis frequency response has a large peak in a very narrow bandwidth around the resonant frequency. This implies that any movement of the peak due to temperature change or other variations might result in a

radical change in gyroscope sensitivity. Thus, the open-loop mode of operation has very poor scale factor stability. To increase the scale factor stability, a quality factor needs to be reduced, but this reduces sensitivity as well.

The importance of quadrature error in MEMS gyroscope performance degradation has been pointed out in the literature [2,8]. Because its effect on the sense axis response is typically a few orders magnitude larger than that of the Coriolis acceleration, it may cause saturation, limit dynamic range and even result in drive mode instability. The detrimental effect of the asymmetric damping term d_{xy} on gyroscope performance has not been considered by many researchers so far. However, its effect should not be underestimated either [9].

3.2 Control Issues

In order to achieve ideal performance in the open loop mode of operation, some control issues arise, aside from the manufacturing issues. These include how to compensate fabrication errors and maintain an ideal operation environment for the open-loop mode of operation.

The control in the open-loop mode of operation may be divided into two tasks. The first is the basic task of the drive axis (*x*-axis) control. The role of this controller is to initiate an oscillation along the drive axis, until a pure oscillation at the resonant frequency ω_x is reached, and to keep the oscillation amplitude constant. Maintaining a constant amplitude of oscillation is necessary to maintain consistent system behavior. This task is typically done by a trans-resistance amplifier configured in positive feedback. The oscillation amplitude can be kept constant using a so-called automatic gain control (AGC) loop [2].

The other control task is to enhance the open-loop mode of operation by realizing an ideal operation environment. This includes compensating major fabrication imperfections such as a quadrature error, and achieving the necessary resonance mode tuning between drive and sense axis frequencies. As state in equation (6), mode-matching of drive and sense resonance frequencies directly affects the scale factor stability of the gyroscope. Automatic

control scheme to null out quadrature error and to tune the mode has not been proposed yet in the literature. These tasks are done manually at the initial calibration stage.

3.3 Off-line Self Calibration Scheme

The on-line identification and compensation of all major fabrication imperfections and their variations is highly desirable to achieve robust and high performance gyroscope operation. To pursue its possibility, let us consider the steady state response of the sense axis dynamics. Assuming a perfect operation of the drive axis and no asymmetric damping, from equation (5), the steady state responses of the sense axis is given by

$$y(t) = y_{Cori}(t) + y_{quad}(t) \tag{8}$$

where

$$y_{Cori}(t) = -X_0 \omega_n \Omega_{z0} G_{Cori\pm} \cos\left((\omega_x \pm \delta)t + \phi_{Cori\pm}\right)$$

$$y_{quad}(t) = -\omega_{xy} X_0 G_{quad} \sin(\omega_x t + \phi_{quad})$$

and

$$G_{Cori\pm} = \frac{1}{\sqrt{\left(\frac{(\omega_x \pm \delta)\omega_y}{Q_y}\right)^2 + \left(\omega_y^2 - (\omega_x \pm \delta)^2\right)^2}}$$

$$\phi_{Cori\pm} = -\arctan 2\ \left(Q_y(\omega_y^2 - (\omega_x \pm \delta)^2),\ \ (\omega_y \pm \delta)\omega_x\right)$$

$$G_{quad} = \frac{1}{\sqrt{\left(\frac{\omega_x \omega_y}{Q_y}\right)^2 + \left(\omega_y^2 - \omega_x^2\right)^2}}$$

$$\phi_{quad} = -\arctan 2\ \left(Q_y(\omega_y^2 - \omega_x^2),\ \ \omega_x \omega_y\right)$$

Thus, the response of the *y*-axis dynamics is a superposition of the responses due to the Corioils acceleration and quadrature error. The response of the Coriolis acceleration is a

dual side band signal centered on the drive axis frequency, and that of quadrature error is a signal concentrated on the drive axis frequency. Both have 90^o phase difference in terms of carrier frequency ω_x. If we can measure the phase ϕ_{quad} and have knowledge of the quality factor Q_y, then the on-line identification and compensation of the quadrature error as well as mode tuning may be possible. However, since this is not a realistic assumption, we propose an off-line self-calibration scheme which identifies ω_y, ω_{xy} and Q_y as the alternative. Although this scheme does not work in an on-line fashion, it can be used at the initial calibration stage when the gyroscope is turned on, or at regular calibration sessions which may be performed periodically.

The proposed self-calibration scheme is composed of two steps. The first step is a mode tuning and the second step consists in the identification of the quality factor and quadrature error.

To achieve mode tuning, consider the condition of no angular motion, i.e. $\Omega_z = 0$, then from equation (8), the steady state *y*-axis displacement becomes a single frequency response. Therefore, it is possible to measure its phase delay with respect to the drive axis displacement signal. The phase delay is given by

$$\begin{aligned} \phi &= -\arctan 2\ \left(Q_y(\omega_y^2 - \omega_x^2),\ \ \omega_x\omega_y\right) \\ &= \arctan 2\ \left(\omega_x\omega_y,\ \ Q_y(\omega_y^2 - \omega_x^2)\right) - 90^0 \end{aligned} \tag{9}$$

If we denote the frequency differences between two modes as ω_d, which must be controlled to zero for mode matching, i.e. $\omega_d = \omega_y - \omega_x$, then, the equation (9) can be written as

$$\phi = \arctan 2\ \left((\omega_x^2 + \omega_x\omega_d),\ \ Q_y(2\omega_x\omega_d + \omega_d^2)\right) - 90^0 \tag{10}$$

The derivative of phase with respect to ω_d is

$$\frac{\partial \phi}{\partial \omega_d} = \cos^2(\phi + 90) \frac{Q_y \omega_x \left(2\omega_x^2 + 2\omega_x \omega_d + \omega_d^2\right)}{\left(\omega_x^2 + \omega_x \omega_d\right)^2} \tag{11}$$

which has always a positive value. Define the phase error as $\tilde{\phi} = \phi + 90$, and consider the positive definite function (PDF) $V = \frac{1}{2}\tilde{\phi}^2$. Then, the time derivative of the V is

$$\dot{V} = \tilde{\phi}\dot{\phi} = \tilde{\phi} \frac{\partial \phi}{\partial \omega_d} \dot{\omega}_d \tag{12}$$

If we choose the frequency adaptation law as

$$\dot{\omega}_d = -\gamma_\omega \tilde{\phi} \tag{13}$$

then

$$\dot{V} = -\gamma_\omega \frac{\partial \phi}{\partial \omega_d} \tilde{\phi}^2 = -2\gamma_\omega \frac{\partial \phi}{\partial \omega_d} V < 0$$

where γ_ω is a positive adaptation gain. Therefore, with the adaptation law (13), the phase delay asymptotically converges to 90^o, and the sense axis frequency is matched to the drive axis frequency. In reality, the adaptation law (13) is realized by adjusting the voltage across the fixed electrodes V_0. Notice that the effective resonant frequency of the *y*-axis is given by the mechanical and negative electrostatic spring constants:

$$\omega_y = \sqrt{\frac{\left(k_{yy} - 2\varepsilon_0 z_0 x_0 \frac{V_0^2}{y_0^3}\right)}{m}} \tag{14}$$

where x_0 and y_0 are respectively the initial equilibrium x-axis position and a nominal capacitive gap, z_0 is the thickness of the electrode, and ε_0 is permittivity of air.

Therefore, the adaptation law (13) is realized by the following nonlinear voltage adaptation law,

$$\dot{V}_0 = \gamma_\omega \tilde{\phi} \frac{m\ y_0^3}{2\varepsilon_0 z_0 x_0 V_0} \sqrt{\frac{\left(k_{yy} - 2\varepsilon_0 z_0 x_0 \frac{V_0^2}{y_0^3}\right)}{m}} \tag{15}$$

Figure 2 shows a typical time domain response of the proposed mode tuning control. For simulation purposes, we made the sense axis resonant frequency to have $+3\%$ deviation

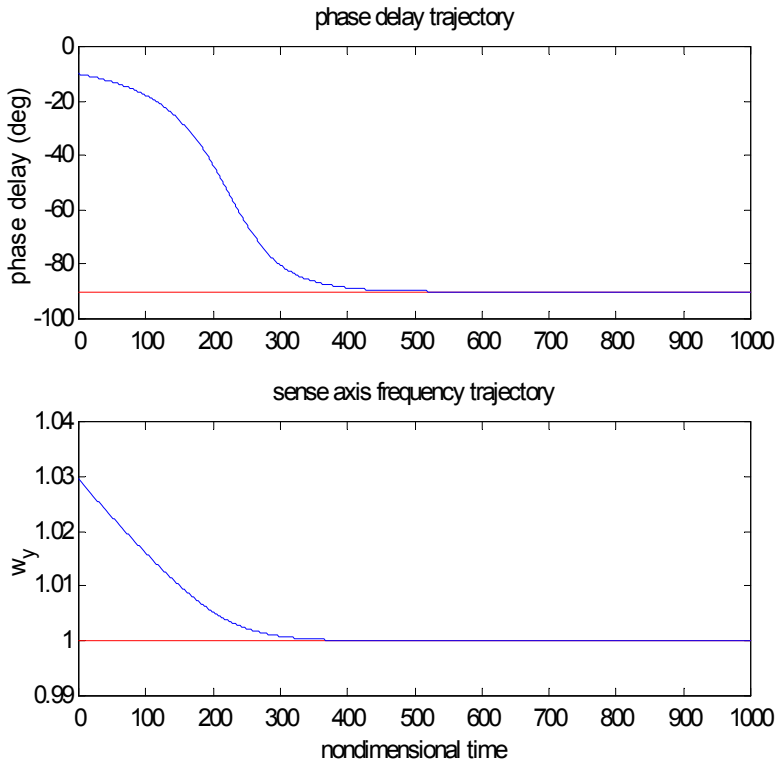

Figure 2. A mode tuning control time response

from the drive axis frequency. This simulation shows that the proposed mode tuning control guarantees that the sense axis frequency will be asymptotically matched to the drive axis frequency.

After the mode tuning step, identifying quality factor (or equivalently scale factor) and the quadrature error are easily performed. Assuming a known and constant angular rate Ω_{z0}, equation (8) becomes

$$y = -\frac{2X_0 Q_y}{\omega_x}\Omega_{z0}\sin(\omega_x t) + \frac{X_0 Q_y}{\omega_x^2}\omega_{xy}\cos(\omega_x t) \tag{16}$$

After demodulating the *y*-axis displacement by $\sin(\omega_x t)$ and $\cos(\omega_x t)$, and decoupling them to the DC response through a low-pass filter, $F_{LPF}(s)$, for y_{Cori} and y_{quad}, we have followings:

$$y_{Cori} = F_{LPF}\left(y\cdot\sin(\omega_x t)\right) = -\frac{X_0 Q_y}{\omega_x}\Omega_{z0}$$

$$y_{quad} = F_{LPF}\left(y\cdot\cos(\omega_x t)\right) = \frac{X_0 Q_y}{2\omega_x^2}\omega_{xy}$$

Thus, the values of Q_y and ω_{xy} are estimated as follows.

$$\hat{Q}_y = \frac{|y_{Cori}|\omega_x}{X_0\Omega_{z0}}$$

$$\hat{\omega}_{xy} = \frac{2|y_{quad}|\omega_x^2}{X_0\hat{Q}_y} = \frac{|y_{quad}|}{|y_{Cori}|}2\omega_x\Omega_{z0}$$

The estimated signal of quadrature error, $\hat{\omega}_{xy}$, can be used to compensate the effect of quadrature error during the operation using the following feedforward control.

$$\tau_y = \hat{\omega}_{xy}X_0\sin(\omega_x t) \tag{17}$$

3.4 Performance Expectation

The main advantage of open-loop mode of operation is that circuitry used for the operation of gyroscope in this mode is simpler than in other modes, since there is no control action in the sense axis. Thus, this mode can be implemented relatively easily and cheaply. The open-loop operational gyroscope also has the possibility to achieve a high resolution if fabrication and other deterministic errors can be perfectly compensated, although it has small dynamic range and bandwidth. This is because it utilizes noiseless mechanical amplification (*Q*-factor) and uses a moderate dynamic sensing circuit. This subsection discusses the expected performance of the open-loop mode in terms of a bandwidth and resolution, and describes some design requirements on the gyroscope parameters such as a mass, spring constants and quality factors for better performance.

Suppose that the sense axis frequency is matched to the drive axis frequency and quadrature error is also ideally compensated through calibration. Asymmetric damping is assumed to be not present. Then, with consideration of a Brownian and sensing noise, equation (5) becomes,

$$\begin{aligned} &\ddot{y} + \frac{\omega_n}{Q_y}\dot{y} + \omega_n^2 y = -2\Omega_{z0}\cos(\delta t) X_0 \omega_n \cos(\omega_n t) + b \\ &\breve{y} = y + n \\ &b \sim (0, S_b), \quad n \sim (0, S_p) \end{aligned} \tag{18}$$

where b is Brownian noise and n is position sensing noise. The analysis of the stochastic properties of the sensing noises, as well as the estimation of their intensity is given in [2,3], and only results are presented here. The estimated power spectral density of the position sensing noise S_p is given by

$$S_p = \left(\frac{2C_0 + C_p}{2V_0 \dfrac{dC}{dy}} \right)^2 4k_B T R_{wire} \tag{19}$$

where k_B, C_p, C_0, R_w and T are respectively Boltzmann's constant, the device's parasite capacitance, nominal sensing capacitance, wiring resistance and absolute temperature.

Brownian noise is a thermal noise that is produced by the collisions between air molecules and the structure, or by viscoelastic effects in the suspension of the gyroscope, and enters to the system as a noisy force generator. Brownian noise can also be modeled as a zero-mean white noise and its power spectral density is given by $S_b = \dfrac{4k_B T d}{m^2}$ [2,3], where m is the mass of the proof mass, and d is a damping coefficient.

The steady state response of equation (18) is

$$y_{Cori}(t) = -X_0 \omega_n \Omega_{z0} G_{Cori\pm} \cos\left((\omega_n \pm \delta)t + \phi_{Cori\pm}\right) + y_w \tag{20}$$

and

$$y_w \sim (0,\ \frac{2k_B T}{m\omega_y^2})$$

$$G_{Cori\pm} = \frac{1}{\sqrt{\left(\dfrac{(\omega_n \pm \delta)\omega_n}{Q_y} \right)^2 + \left(\omega_n^2 - (\omega_n \pm \delta)^2\right)^2}}$$

$$\phi_{Cori\pm} = -\arctan 2\ \left(Q_y(\omega_n^2 - (\omega_n \pm \delta)^2),\ \ (\omega_n \pm \delta)\omega_n\right)$$

To compute the bandwidth of the open loop mode, ω^* is calculated such that $\dfrac{G_{Cori}(\omega^*)}{G_{Cori}(\omega_n)} = \dfrac{1}{\sqrt{2}}$ and $\phi_{Cori}(\omega^*) = \mp 45^o$, then

$$\omega^* = \omega_n \sqrt{1+\left(\frac{1}{2Q_y}\right)^2} \mp \frac{\omega_n}{2Q_y}$$

In case of $Q_y \geq 10$, the factor $\sqrt{1+(1/2Q_y)^2} \approx 1$ and $\omega^* = \omega_n \mp \omega_n / 2Q_y$. Therefore, the bandwidth is given by $\frac{\omega_n}{2Q_y}$. The bandwidth of the open loop mode is determined by the gyroscope's resonant frequency and quality factor. From the static scale factor equation (7) and the power spectral density of the position measurement (19), the position sensing noise equivalent angular rate can be computed as

$$\overline{\Omega}_z = \frac{\sqrt{S_p}}{X_0} BW^2 = \frac{\sqrt{S_p}}{X_0}\left(\frac{\omega_n}{2Q_y}\right)^2 \tag{21}$$

where *BW* is a gyroscope bandwidth and it is assumed that an ideal low-pass filter is used in the demodulation process. The Brownian noise floor equivalent angular rate is roughly given by [2]

$$\overline{\Omega}_z \approx \sqrt{\frac{2k_B T}{mQ_y X_0^2 \omega_n}} \tag{22}$$

Equation (22) is an important design rule for determining the ultimate achievable resolution of the open-loop mode operational gyroscope. On the other hand, equation (21) defines actual achievable resolution by considering position sensing circuitry noise. Equations (21) and (22) suggest that, the higher the quality factor and the larger the mass, the better the resolution of the gyroscope. However, the resonant frequency should be selected depending on the position sensing circuit technology. As technology is further developed so that readout noise is made sufficiently small, a large resonant frequency will be better choice in terms of achieving large bandwidth and high resolution.

4. Closed-loop Mode of Operation

4.1 Strategy and Previous Work

In contrast to the open-loop mode of operation where there is no feedback control actions on the sense axis of the gyroscope, in the closed-loop mode of operation, feedback control is applied to the sense axis, as well. In this mode, the sense amplitude of oscillation is continuously monitored and driven to zero. As a consequence, the bandwidth and dynamic range of the gyroscope can be greatly increased beyond what can be achieved with the open-loop mode of operation. However, the effect of the asymmetric damping term is not distinguishable from the Coriolis acceleration term. Thus, this term still creates an inherent ZRO as in the case of the open-loop mode of operation.

Although many authors have commented on the need of closed loop control, few published papers present specific designs. Two types of controllers have been proposed in the literature. One is Kalman filter based preview control [5] and the other is a force-balancing feedback control strategy, which uses a sigma-delta modulation [6].

The Kalman filter based preview control approach requires that a quadrature error compensation control be first implemented using a separate control loop. Using the well-known separation principle, an LQ regulator and a Kalman filter based on equation (5) can be designed independently. The actual gyroscope output is the angular rate estimate, $\hat{\Omega}_z$, which is one of the state of the Kalman filter. The bandwidth of this gyroscope is set by the Kalman filter dynamics, which is usually fast. In spite of these benefits, the closed loop system may be unstable or produce a large bias error in the angular rate estimate, when the exact values of the quality factor, drive and sense axis resonant frequencies are unknown, because the LQG control is not robust to parameter uncertainties.

The force-balancing control strategy was originally developed for MEMS accelerometers control [10], where it has been successfully applied, and it has been extended to MEMS

gyroscopes. The basic idea behind the force-balancing control strategy is that, if the sense mode amplitude is regulated to zero by feedback control action, then, since $\ddot{y} \cong \dot{y} \cong y \cong 0$, equation (5) yields in steady-state response,

$$\tau_y = \omega_{xy} x + (d_{xy} + 2\Omega_z)\dot{x} \tag{23}$$

This implies that applied angular rate Ω_z can in principle be inferred from the sense axis control output τ_y, under the assumption that $d_{xy} = 0$.

4.2 Force-balancing Control

The force-balancing control strategy requires that the sense axis closed loop system be robust to parameter uncertainties and variations, and have minimal phase shift so that the response of the system to the Coriolis acceleration and quadrature error can be distinguishable. A block diagram of a sense axis force-balancing control is shown in Figure 3. $G(s)$ is the sense axis gyroscope dynamics, $K(s)$ is the compensator which will be subsequently designed, $r = -2\Omega_z X_0 \omega_x \cos(\omega_x t) - \omega_{xy} X_0 \sin(\omega_x t)$ is the modulated input signal resulting from the Coriolis acceleration and quadrature error, $u = \tau_y$ is the control output, n is the measurement noise, and b is the Brownian input noise. Figure 3 also includes a demodulation block, which will be defined subsequently.

The closed loop sensitivity transfer functions for u and y are given by

$$\begin{aligned} u(s) &= T(s)(r+b) + S(s)n \\ y(s) &= V(s)(r+b) - T(s)n \end{aligned} \tag{24}$$

where $T(s) = \dfrac{K(s)G(s)}{1+K(s)G(s)}$, $S(s) = \dfrac{K(s)}{1+K(s)G(s)}$ and $V(s) = \dfrac{G(s)}{1+K(s)G(s)}$. The control design goal is to flatten the gain of the complementary sensitivity function for *u* around the drive axis frequency ω_x, i.e.

$$\left|T(j\omega)\right| \approx const \quad \text{for}\, \omega \in [\omega_x - \Delta\omega,\ \ \omega_x + \Delta\omega]$$

The compensator $K(s)$ may be designed by various methods such as μ-synthesis and H^∞ for stability robustness, or using classical control synthesis techniques.

If the magnitude of the closed loop complementary transfer function from the angular rate to the control output is flat around the drive axis frequency, the gyroscope's scale factor will remain constant in the presence of drive or sense axis frequency variations. Moreover, the gyroscope's bandwidth can be increased up to the drive axis frequency. The dynamic range and linearity are also improved to the extent of the control authority, since the sensitivity transfer function from the angular rate to the sense axis displacement is almost zero. Since, by equation (24), the steady-state control signal *u* contains both the Coriolis and quadrature error signals, a demodulation is needed for extracting angular velocity information from the control signal. Eventually, the overall gyroscope performance will depend on the demodulation method used.

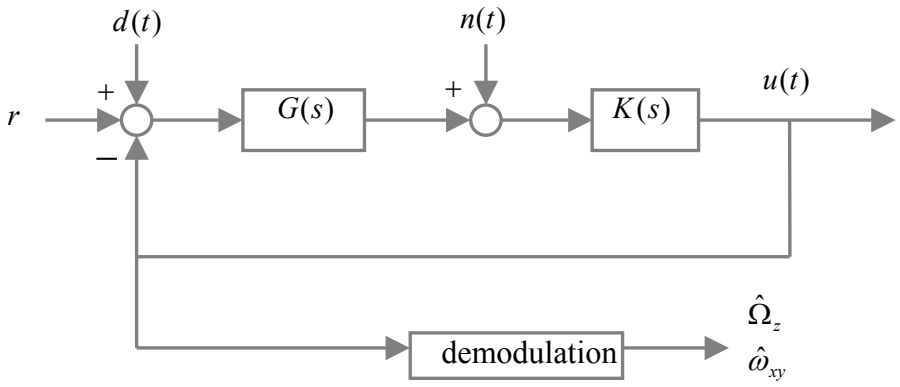

Figure 3. Block diagram of the force-balancing control

The steady state response of the control output of equation (24) is given by

$$u(t) = u_{Cori}(t) + u_{quad}(t) + u_w(t) + u_n(t) \tag{25}$$

where

$$u_{Cori}(t) = -X_0 \omega_x \Omega_{z0} T_{Cori\pm} \cos\left((\omega_x \pm \delta)t + \phi_{Cori\pm}\right)$$

$$u_{quad}(t) = -\omega_{xy} X_0 T_{quad} \sin(\omega_x t + \phi_{quad})$$

$$u_w \sim (0, \sigma_w^2), \;\; u_n \sim (0, \sigma_n^2)$$

and

$$T_{Cori\pm} = \left|T(s)\right|_{s=j(\omega_x \pm \delta)}, \; T_{quad} = \left|T(s)\right|_{s=j\omega_x}$$

$$\phi_{Cori\pm} = \angle\left(T(s)\right)_{s=j(\omega_x \pm \delta)}, \; \phi_{quad} = \angle\left(T(s)\right)_{s=j\omega_x}$$

$$\sigma_w^2 = \int \left|T(j\omega)\right|^2 S_{br} d\omega, \; \sigma_n^2 = \int \left|S(j\omega)\right|^2 S_p d\omega$$

where it is assumed that $\Omega_z = \Omega_{z0} \cos(\delta\, t)$. Suppose that the phase delay is small, i.e. $\phi_{Cori,quad} \approx 0$ around the anticipated drive frequency region. Then, the angular rate and quadrature error may be demodulated from the control output by multiplying this signal by $\cos(\omega_x t)$ and $\sin(\omega_x t)$, and filtering the resulting signals with a low-pass filter. The demodulated signals become

$$\begin{aligned}
\hat{\Omega}_z &= F_{LPF}\left(u(t) \cdot \cos(\omega_x t)\right) \\
&= -\frac{1}{2} X_0 \omega_x T_{Cori\pm} \Omega_{z0} \cos(\pm\delta t + \phi_{Cori\pm} + \phi_{LPF}) \\
&\quad -\frac{1}{2} X_0 \omega_{xy} T_{quad} \sin(\phi_{quad}) + u_{wf} + u_{nf} \\
\hat{\omega}_{xy} &= F_{LPF}\left(u(t) \cdot \sin(\omega_x t)\right) \\
&= \frac{1}{2} X_0 \omega_x T_{Cori\pm} \Omega_{z0} \sin(\pm\delta t + \phi_{Cori\pm} + \phi_{LPF}) \\
&\quad -\frac{1}{2} X_0 \omega_{xy} T_{quad} \cos(\phi_{quad}) + u_{wf} + u_{nf}
\end{aligned}$$

where ϕ_{LPF} is the phase delay due to the low-pass filter, $u_{wf} = F_{LPF}(\cos(\omega_x t) \cdot u_w)$ and $u_{nf} = F_{LPF}(\cos(\omega_x t) \cdot u_n)$. Notice however that, unless the ϕ_{quad} is exactly zero, the estimation of angular rate is contaminated by the unknown quadrature error coupling term ω_{xy}. Unfortunately, usually the quadrature error is 3 or 4 orders of magnitude larger than the angular rate. Although the quadrature error term can potentially be canceled out by initial calibration, it may vary during the operation of the gyroscope. In the force-balancing approach, sense and drive resonance frequency mis-match is not as critical a problem as is in the open-loop operation, unless the gyroscope closed-loop bandwidth is much larger than in the open-loop mode. When high resolution is required, resonant mode matching is important to attain a consistent resolution performance. However, in this case the bandwidth of the gyroscope will be small. This is also the case in the open-loop mode, where mode matching is important in order to attain a consistent scale factor. However, as opposed to the open-loop operation mode, it is very difficult to tune the sense axis resonant frequency, since phase information for mode matching is lost in closed-loop operation mode.

4.3 Adaptive Add-On Control

We investigate the use of an adaptive algorithm for estimating angular rate and at the same time, identifying and compensating quadrature error, and possible attaining mode match in an on-line fashion. Note that the effect of variations in drive or sense axis frequencies is not observed explicitly in the control output of a conventional force-balancing system. The idea behind the use of adaptive add-on control is to make the nominal control output of the conventional force-balancing system equal to zero by adding an additional outer loop. The add-on control outer loop is composed of a band-pass filter, a parameter adaptation law and a modulation term. Figure 4 shows a block diagram of force-balancing system with the adaptive add-on control.

The modulated input signal r in the equation (24) is re-written in regressor form as

$$r = -2\Omega_z \dot{x} - \omega_{xy} x = -\theta^T v \tag{26}$$

where $\theta = [2\Omega_z \ \ \omega_{xy}]^T$ is assumed to be an unknown parameter and $v = [\dot{x} \ \ x]^T$ is the measurable regressor. Suppose that the input signal r is estimated by a parameter adaptation algorithm, then its estimate signal and errors are

$$\begin{aligned} \hat{r} &= -2\hat{\Omega}_z(t)\dot{x} - \hat{\omega}_{xy}(t)x = -\hat{\theta}^T v \\ \tilde{r} &= r - \hat{r} = 2\tilde{\Omega}_z(t)\dot{x} + \tilde{\omega}_{xy} x = \tilde{\theta}^T v \end{aligned} \tag{27}$$

where the parameter estimate errors are $\tilde{\Omega}_z = \hat{\Omega}_z - \Omega_z$, $\tilde{\omega}_{xy} = \hat{\omega}_{xy} - \omega_{xy}$ and $\tilde{\theta} = \hat{\theta} - \theta$.

The control error dynamics $\tilde{u}$ is

$$\begin{aligned} \tilde{u} &= T(r + d - \hat{r}) + S(n) \\ &= T(\tilde{\theta}^T v) + T(d) + S(n) \end{aligned} \tag{28}$$

If the error signal $\tilde{u}$ passes through a band-pass filter $F_{BPF}(s)$, then

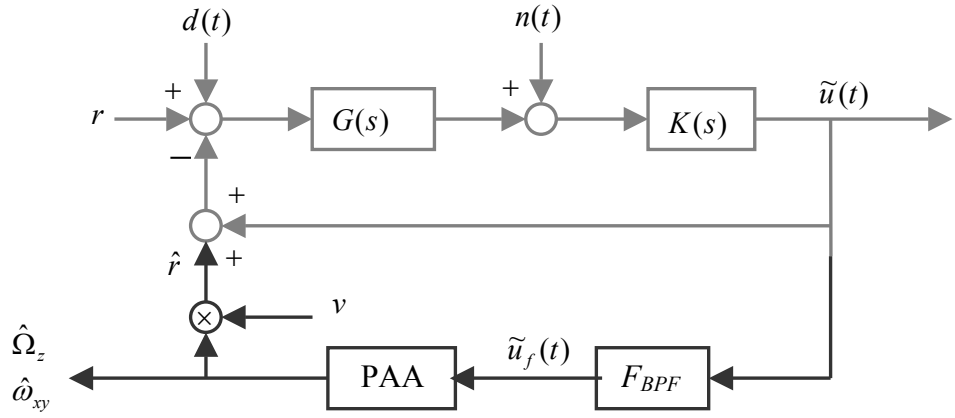

Figure 4. Block diagram of the adaptive add-on control

$$\begin{aligned}\tilde{u}_f &= F_{BPF}(\tilde{u}) \\ &= T_{BPF}\left(\tilde{\theta}^T v\right) + T_{BPF}(d) + S_{BPF}(n)\end{aligned} \tag{29}$$

where $T_{BPF}(s) = F_{BPF}(s)T(s)$ and $S_{BPF}(s) = F_{BPF}(s)S(s)$.

The following theorem holds.

Theorem

Assume that Ω_z and ω_{xy} are constant. Suppose that a conventional force-balancing closed loop system is stable with a controller $K(s)$. If a band-pass filter is designed such that the phase delay from the modulated input signal r to the output of a band-pass filter is less than 90^0 for a drive axis frequency ω_x, and the parameter estimates $\hat{\Omega}_z$ and $\hat{\omega}_{xy}$ are updated by the following adaptation laws:

$$\begin{aligned}\dot{\hat{\Omega}}_z &= -\gamma_\Omega \tilde{u}_f \dot{x} \\ \dot{\hat{\omega}}_{xy} &= -\gamma_\omega \tilde{u}_f x\end{aligned} \tag{30}$$

then the angular rate Ω_z and quadrature error ω_{xy} can be estimated correctly, i.e. $\tilde{\Omega}_z \to 0$, $\tilde{\omega}_{xy} \to 0$, where γ_Ω and γ_ω are positive adaptation gains.

Proof:

Since the propagation equation of the stochastic expectation has the same form as the deterministic counterpart, we can consider the deterministic case, i.e. $b = 0$ and $n = 0$. Usually, T(s) and $T_{BPF}(s)$ are not SPR (strictly positive real), so it is difficult to prove the stability of the closed-loop system with an adaptation loop. Here, we make use of the fact that the driving signal is a single frequency sinusoid, and take an averaging approach [11]. Assuming that the applied angular rate and quadrature error are constant, then equation (30) is equal to

$$\dot{\tilde{\theta}} = -\begin{bmatrix} 2\gamma_\Omega & 0 \\ 0 & \gamma_\omega \end{bmatrix} \begin{bmatrix} X_0 \omega_x \cos(\omega_x t) \\ X_0 \sin(\omega_x t) \end{bmatrix} \tilde{u}_f \tag{31}$$

Assuming that estimate error dynamics $\tilde{\theta}$ is slow, from equation (29), the steady state dynamics of $\tilde{u}_f$ is approximately given by

$$\begin{aligned} \tilde{u}_f &\approx T_{BPF}\left(v^T\right)\tilde{\theta} \\ &= \left|T_{BPF}(\omega_x)\right| [X_0 \omega_x \cos(\omega_x t + \phi) \;\; X_0 \sin(\omega_x t + \phi)]\, \tilde{\theta} \end{aligned} \tag{32}$$

where ϕ is a phase delay from the modulated input signal r to the output of the band-pass filter. Substituting (32) into (31) and taking averages result in

$$\begin{bmatrix} \dot{\tilde{\Omega}}_z \\ \dot{\tilde{\omega}}_{xy} \end{bmatrix}_{AVG} = -\left|T_{BPF}(\omega_x)\right| X_0^2 R_{\Omega\omega} \begin{bmatrix} \tilde{\Omega}_z \\ \tilde{\omega}_{xy} \end{bmatrix}_{AVG} \tag{33}$$

where

$$R_{\Omega\omega} = \begin{bmatrix} \gamma_\Omega \omega_x^2 \cos\phi & -\gamma_\Omega \omega_x \sin\phi \\ \frac{1}{2}\gamma_\omega \omega_x \sin\phi & \frac{1}{2}\gamma_\omega \cos\phi \end{bmatrix}$$

We have used the fact that the products of sinusoids at different frequencies have zero average. A sufficient condition for the system in the equation (33) to be asymptotically stable is that the cross-correlation matrix $R_{\Omega\omega}$ be positive-definite. This is achieved if $\cos\phi > 0$. Therefore, if $-90^0 < \phi < 90^0$, the convergence of parameter errors to zero is guaranteed, and the stability of the system is proven.

If we carefully design a compensator $K(s)$ and a band-pass filter $F_{BPF}(s)$ so that phase delay is as small as possible, the angular rate estimate dynamics will be almost decoupled from that of the quadrature error estimate. In this case, the quadrature error estimation transient response will not significantly affect the transient response of the angular rate estimate and vice versa. Although the quadrature error estimate dynamics affects that of the angular rate estimate, this only happens during the transient period. This is the main advantage of this scheme over the conventional force-balancing control, where the angular rate estimate is contaminated by the quadrature error term, unless it is perfectly compensated.

4.4 Performance Expectation

The bandwidth of a conventional force-balancing controlled gyroscope is defined by the cut-off frequency of the low-pass filter used in the demodulation process. On the other hand, the bandwidth of the proposed force-balancing controlled gyroscope with adaptive add-on control is defined by the adaptation gain γ_Ω. From equation (33), assuming that $\phi \approx 0$, its bandwidth can be estimated by

$$BW \approx \gamma_\Omega \left|T_{BPF}(\omega_x)\right| X_0^2 \omega_x^2 \tag{34}$$

Of course, the actual maximum bandwidth is also limited by the band-pass filter. Therefore, the adaptation gain γ_Ω should be selected so that the bandwidth estimate given by equation (34) is lower than half of the frequency pass-band of the band-pass filter.

The ideal resolution of a conventional force-balancing gyroscope is defined by

$$\sigma = \frac{1}{X_0 \omega_x \left|T(\omega_x)\right|} \left(\int_{BW-\omega_x}^{BW+\omega_x} \left|T(j\omega)\right|^2 S_b \, d\omega + \int_{BW-\omega_x}^{BW+\omega_x} \left|S(j\omega)\right|^2 S_p \, d\omega \right)^{\frac{1}{2}} \tag{35}$$

In reality, the actual sharpness of the low-pass filter in the demodulation process and aliasing affect resolution performance, and it may be much worse than the estimate given by equation (35). In the case of the adaptive add-on control, resolution is a function of the adaptation gain γ_Ω and the pass-band of the band-pass filter $F_{BPF}(s)$. In order to accurately estimate resolution of nominal system, consider the following state-space realization of $T_{BPF}(s)$ and $S_{BPF}(s)$:

$$T_{BPF}(s): \ (A_T, B_T, C_T)$$
$$S_{BPF}(s): \ (A_S, B_S, C_S)$$

Then, the equations (29) and (30) are realized the following state-space form.

$$\begin{bmatrix} \dot{x}_e \\ \dot{\tilde{\theta}} \end{bmatrix} = \begin{bmatrix} A_{11} & A_{12} \\ A_{21} & 0 \end{bmatrix} \begin{bmatrix} x_e \\ \tilde{\theta} \end{bmatrix} + \begin{bmatrix} B_1 \\ 0 \end{bmatrix} \begin{bmatrix} b \\ n \end{bmatrix} \tag{36}$$

where

$$A_{11} = diag\{A_T, A_T, A_S\}, \ A_{21} = -\gamma v \ [C_T \ \ C_T \ \ C_s]$$

$$A_{12} = \begin{bmatrix} B_T v^T \\ 0 \\ 0 \end{bmatrix}, \ B_1 = \begin{bmatrix} 0 & 0 \\ B_T & 0 \\ 0 & B_S \end{bmatrix}$$

$$\gamma = diag\{2\gamma_\Omega, \gamma_\omega\}, \ v = [\dot{x} \quad x]^T$$

The covariance of $[x_e^T \ \tilde{\theta}^T]^T$ can be computed by solving the following covariance propagation equation.

$$\dot{\boldsymbol{P}} = \boldsymbol{P}\boldsymbol{A}^T + \boldsymbol{A}\boldsymbol{P} + \boldsymbol{B}\boldsymbol{S}\boldsymbol{B}^T \tag{37}$$

where $\boldsymbol{S} = diag\{S_b, S_p\}$, and $E[\cdot]$ denotes stochastic expectation. The standard deviation of the angular rate estimate error, or resolution σ_Ω, is obtained from the covariance matrix $\boldsymbol{P}$, and is computed by

$$\sigma_\Omega = \sqrt{\boldsymbol{C}\boldsymbol{P}_o\boldsymbol{C}^T} \tag{38}$$

where $\boldsymbol{C} = [0_{1\times *}\ 1]$.

Now, we investigate a relationship of resolution performance between conventional force-balancing and adaptive add-on force-balancing schemes. If we substitute equation (29) to (31), then

$$\dot{\tilde{\theta}} = -\gamma v T_{BPF}(v^T\tilde{\theta}) - \gamma v T_{BPF}(d) - \gamma v S_{BPF}(n) \tag{39}$$

The stochastic expectation equation of (39) is given by $E[\dot{\tilde{\theta}}] = -\gamma v T_{BPF}(v^T E[\tilde{\theta}])$. Define the expectation error as $\breve{\theta} = \tilde{\theta} - E[\tilde{\theta}]$, then

$$\begin{aligned}\dot{\breve{\theta}} &= -\gamma v T_{BPF}(v^T\breve{\theta}) - \gamma v T_{BPF}(d) - \gamma v S_{BPF}(n)\\ &\approx -\gamma v T_{BPF}(v^T)\breve{\theta} - \gamma v T_{BPF}(d) - \gamma v S_{BPF}(n)\end{aligned} \tag{40}$$

where we have utilized the assumption that the dynamics $\breve{\theta}$ is slow. Thus, the transfer function from noises to $\breve{\theta}$ is given by

$$\begin{aligned}\breve{\theta}(s) = &-(sI + \gamma v T_{BPF}(v^T))^{-1}\gamma v T_{BPF}(d)\\ &-(sI + \gamma v T_{BPF}(v^T))^{-1}\gamma v S_{BPF}(n)\end{aligned} \tag{41}$$

If we assume phase delay $\phi \approx 0$ and consider only the angular rate part, then equation (41) is simplified as

$$\begin{aligned}\breve{\Omega}_z(s) &\approx -\frac{\gamma_\Omega X_0 \omega_x}{s+\gamma_\Omega X_0^2 \omega_x^2 \left|T_{BPF}(\omega_x)\right|}\cos(\omega_x t)\left(T_{BPF}(d)+S_{BPF}(n)\right) \\ &= -\frac{1}{X_0 \omega_x \left|T_{BPF}(\omega_x)\right|}\frac{BW}{s+BW}\cos(\omega_x t)\left(T_{BPF}(d)+S_{BPF}(n)\right)\end{aligned} \tag{42}$$

Equation (42) can be interpreted as follows: The noise that contaminates the angular rate estimate is a low-pass filtered signal of the demodulated noise signals, passed through shaping filters $T_{BPF}(s)$ and $S_{BPF}(s)$. These are the same noise properties observed in a conventional force-balancing control using a demodulation process. Therefore, equation (35) can be also used to calculate the upper estimate of the resolution for the adaptive add-on controlled gyroscope. Note that the noise properties of the angular rate estimate such as standard deviation can easily be calculated by measuring control output signal $\tilde{u}$. These properties may be used in an automatic mode tuning.

5. Simulation

A simulation study using the preliminary design data of the MIT-SOI MEMS gyroscope was conducted, to test the analytical results and verify the predicted performance of the adaptive add-on controlled gyroscope presented in this report. We assumed that the drive and sense axis resonant frequencies are matched and the magnitude of quadrature error is 0.1% of nominal resonant frequency. The data of some of the gyroscope parameters in the model is summarized in Table 1. Notice that the simulation results are shown in non-dimensional units, which are non-dimensionalized based on the proof-mass, length of one micron and the x-axis nominal natural frequency.

The estimate of the angular rate response to the step input angular rate is shown in Figure 5. In this figure, the upper and lower bounds of the analytically estimated standard deviation are also plotted. The estimated standard deviation with equation (38) is 0.56 deg/sec at 50 Hz of bandwidth. Figure 6 shows the estimate of angular rate response to the sinusoidal

input angular rate, and Figure 7 shows the time response of the quadrature error estimate. These simulation results well match the theoretical results obtained in this report.

parameter	*value*
mass	$5.095x10^{-7}$ kg
x-*axis frequency*	*4.17* KHz
Quality factor	*40*
Brownian noise PSD	$3.68x10^{-24}$ N^2sec
Position noise PSD	$1.49x10^{-27}$ m^2sec

Table 1. Key parameters of the gyroscope

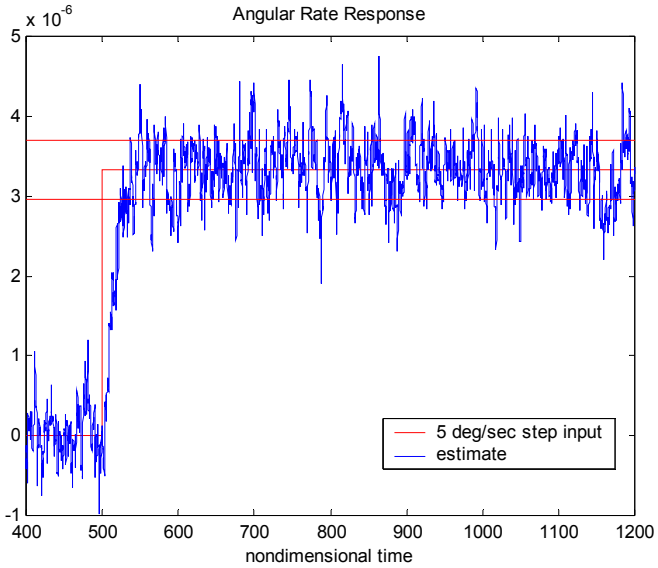

Figure 5. Time responses of angular rate estimate to the 5 deg/sec step input

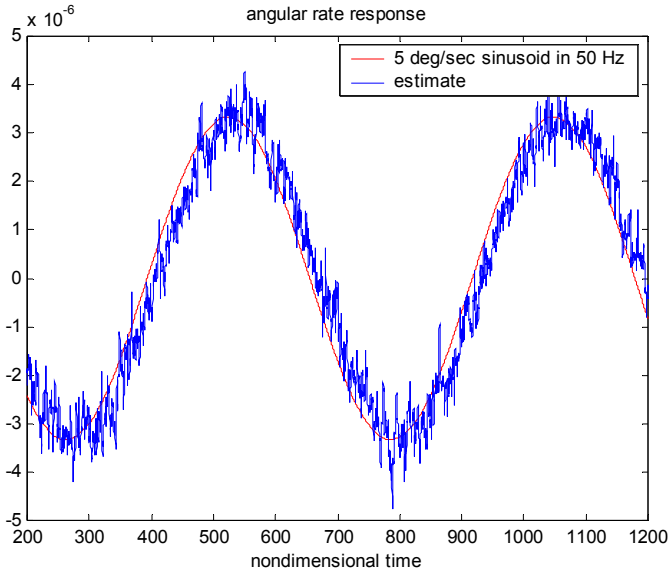

Figure 6. Time responses of angular rate estimate to 5 deg/sec sinusoid input at 50 Hz

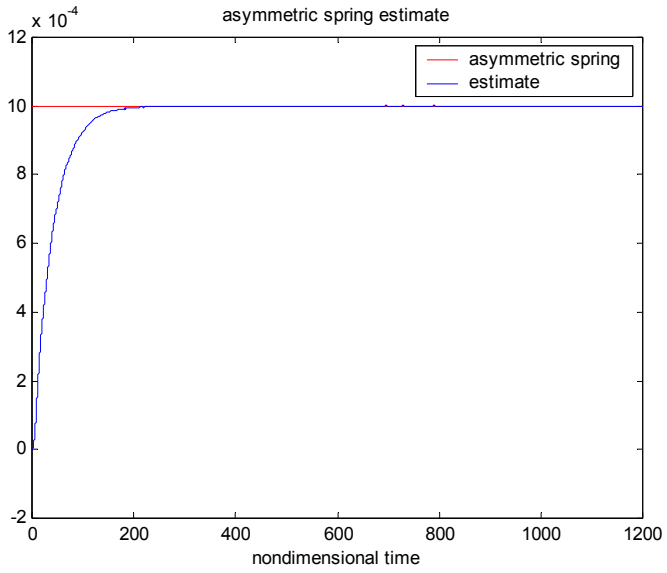

Figure 7. Time response of quadrature error estimate

6. Conclusions

The measurement strategy of both the open-loop and closed-loop modes is based on the same physics, i.e. generating a Coriolis acceleration by driving a proof mass in a constant amplitude oscillation along the drive axis and inducing an oscillation along the sense axis, which is proportional to applied angular rate. The major difference between the closed-loop and open-loop mode of operation lies in that in the former the displacement of the sense axis is controlled to zero, while in the latter it is measured. The benefits of a closed-loop operation are more scale factor stability, higher linearity and higher bandwidth, thus achieving better performance than that in the open-loop mode of operation.

For an open-loop mode of operation, an off-line self-calibration scheme was proposed for estimating fabrication imperfections and enhancing the performance of a gyroscope operating in open-loop mode. This scheme can be implemented during the initial calibration stage when the gyroscope is turned on, or at regular calibration sessions, which may be performed periodically, although this scheme does not work in an on-line fashion.

For a closed-loop mode of operation, an adaptive add-on control scheme was proposed. The idea behind this add-on control is to achieve a zero nominal control output in a conventional force-balancing system by adding an additional outer loop. The proposed outer loop is composed of a band-pass filter, a parameter adaptation algorithm, and an algorithm that generates estimates of the gyroscopic inputs and other perturbation inputs due to fabrication defects. This parameter adaptation algorithm estimates the angular rate and, at the same time, identifies and compensates quadrature error, and may permit on-line automatic mode tuning.

The convergence and resolution analysis of the adaptive add-on controlled gyroscope was presented. This analysis shows that the proposed adaptive add-on control scheme prevents the angular rate estimate from being contaminated by the quadrature error, while keeping ideal resolution performance of a conventional force-balancing scheme.

Simulation results were presented which corroborate the analytically derived performance.

However, both the open-loop and closed-loop modes are inherently sensitive to some types of fabrication imperfections which can be modeled as cross-damping terms, which produce ZRO.

References

[1] Yazdi, N., F. Ayazi and K. Najafi, "Micromachined Inertial Sensors", *Proceedings of the IEEE*, Vol.86, No.8, pp.1640-1659, Aug. 1998.

[2] Clark, W.A., *Micromachined Vibratory Rate Gyroscopes*, Doctoral Thesis, U.C. Berkeley, 1997.

[3] Juneau, T.N, *Micromachined Dual Input Axis Rate Gyroscope*, Doctoral Thesis, U.C. Berkeley, 1997.

[4] Loveday, P.W and C.A. Rogers, "Modification of Piezoelectric Vibratory Gyroscope Resonator Parameters by Feedback Control", *IEEE Transactions on Ultrasonics, Ferroelectrics and Frequency Control*, Vol.45, No.5, pp.1211-1215, Sep. 1998.

[5] Ljung, P.B., *Micromachined Gyroscope with Integrated Electronics*, Doctoral Thesis, U.C. Berkeley, 1997.

[6] Jiang, X., J. Seeger, M. Kraft and B.E. Boser, "A monolithic surface micromachined Z-axis gyroscope with digital output", *2000 Symposium on VLSI Circuits*, Honolulu, HI, USA, pp.16-19, June 2000.

[7] Shkel, A.M., R. Horowitz, A.A. Seshia, S. Park and R.T. Howe, "Dynamics and Control of Micromachined Gyroscopes", *Proceedings of the American Control Conference*, pp.2119-2124, Jun. 1999.

[8] Shkel, A., R.T. Howe and R. Horowitz, "Modeling and simulation of micromachined gyroscopes in the presence of imperfection", *Int. Conf. On Modelling and Simulation of Microsystems,* pp. 605-608, Puerto Rico, U.S.A., 1999.

[9] Park, S., *Adaptive Control Strategies for MEMS Gyroscopes*, Doctoral Thesis, U.C. Berkeley, 2000.

[10] Lu, C. M. Lamkin and B.E. Boser, "A Monolithic Surface Micromachine Accelerometer with Digital Output", *IEEE Journal of Solid-State Circuits*, Vol.30, No.12, pp.1367-1373, Dec. 1995

[11] Sastry, S. S., *Adaptive Control: Stability, Convergence and Robustness*, Prentice Hall, 1989.